Tuijin Jishu/Journal of Propulsion Technology
ISSN: 1001-4055
Vol. 47 No. 04 (2026)

Geotechnical Improvement of Sugarcane Bagasse Ash and Calcium Chloride–Stabilised Expansive Soil Subgrade for Flexible Pavement Applications

T. Sarada[a], **D. Koteswara Rao**[b], **K.V.S.G. Murali Krishna**[c]

[a] Research Scholar, Department of Civil Engineering, University College of Engineering, JNTUK, Kakinada – 533003, Andhra Pradesh, India;

[b] Professor of Civil Engineering & OSD to Hon'ble Vice Chancellor, JNTUK, Kakinada – 533003, Andhra Pradesh, India;

[c] Professor of Civil Engineering, JNTUK, Kakinada – 533003, Andhra Pradesh, India

Abstract

Expansive clays prevalent across peninsular India, particularly the black cotton soils of Telangana, pose serious challenges for flexible pavement subgrade construction on account of their high swell-shrink activity, low bearing capacity, and susceptibility to moisture-induced strength loss. This study investigates a binary stabilisation system comprising sugarcane bagasse ash (SBA) and calcium chloride ($CaCl_2$) for improvement of a highly plastic clay (CH) subgrade sourced from Shankarpally, Telangana (PI = 50.41%, DFS = 90%, soaked CBR = 2.2%). Laboratory tests included standard Proctor compaction, Atterberg limits, differential free swell, soaked California Bearing Ratio (CBR), unconfined compressive strength (UCS), X-ray diffraction (XRD), X-ray fluorescence (XRF), and scanning electron microscopy with energy-dispersive spectroscopy (SEM-EDS). At the optimum dosage of 20% SBA + 1.5% $CaCl_2$ (by dry mass of soil), the treated subgrade achieved a maximum dry density of 1.77 g/cm³ at 16.20% optimum moisture content. Plasticity index declined from 50.41% to 9.30%, differential free swell decreased from 90% to 13%, and soaked CBR increased to 11.20% — a 5.09-fold improvement over the untreated baseline. UCS rose from 0.727 kg/cm² to 1.253 kg/cm². Analytical processing of the results showed a 34.3% reduction in void ratio and a 3.8-fold rise in the estimated subgrade resilient modulus (22 to 83 MPa), and regression models relating DFS to PI, CBR to dry density and PI, and UCS to CBR reproduced the measured values with mean absolute errors of 1.3–9.6%. Microstructural analyses confirmed pozzolanic calcium silicate hydrate (C–S–H) and calcium aluminate hydrate (C–A–H) gel formation, accelerated by the calcium ion supply from $CaCl_2$. The stabilised subgrade satisfies IRC:37–2018 requirements and offers a sustainable, low-carbon alternative for expansive subgrade improvement using agro-industrial and industrial by-products.

Keywords: *Expansive soil stabilisation; Sugarcane bagasse ash; Calcium chloride; Soaked CBR; Differential free swell; Empirical modelling; IRC:37; Sustainable subgrade.*

1. Introduction

Expansive clay soils, characterised by a mineralogy dominated by montmorillonite, undergo substantial volumetric swelling on water absorption and shrinkage on desiccation. These repetitive volumetric changes induce pavement surface heaving, longitudinal and transverse cracking, subgrade softening, and accelerated structural deterioration, leading to disproportionate maintenance expenditure [1], [2]. In India, the black cotton soils of Telangana, Andhra Pradesh, Maharashtra, and Karnataka cover approximately 20% of the national land mass.

Their wide distribution across major highway corridors makes expansive subgrade improvement a high-priority engineering challenge for NHAI and state infrastructure agencies [3], [4].

MoRTH specifications commonly require a minimum soaked CBR of 8% for subgrade acceptance on national and state highways, and IRC:37–2018 requires an effective subgrade CBR above 5% for roads carrying more than 450 commercial vehicles per day. Soils failing this criterion must be either replaced or chemically stabilised. Conventional binders such as ordinary Portland cement (OPC) and lime are effective but carry high embodied-carbon penalties and significant material costs [5]. The imperative to reduce construction-sector carbon emissions has driven growing research interest in industrial and agricultural pozzolanic by-products: pulverised fuel ash [6], ground granulated blast-furnace slag [7], rice husk ash [8], sugarcane bagasse ash (SBA) [9]–[11], and foundry sand with alkali-activated geopolymer [29] have all demonstrated promising stabilisation performance.

Sugarcane bagasse ash is generated as a furnace residue during juice extraction at sugar mills and is available in large quantities at minimal cost. SBA typically contains 59–71% amorphous SiO_2, conferring strong pozzolanic reactivity upon contact with calcium-bearing species [12], [13]. The fundamental stabilisation mechanism involves reaction of SBA-derived reactive SiO_2 and Al_2O_3 with calcium hydroxide present in the pore water, precipitating cementitious calcium silicate hydrate (C–S–H) and calcium aluminate hydrate (C–A–H) gel phases that fill inter-particle voids, increase stiffness, and suppress swell potential [14], [15].

Calcium chloride ($CaCl_2$) is a highly hygroscopic inorganic salt that has long been employed as a soil stabiliser and dust suppressant. In expansive clay systems, $CaCl_2$ operates through two principal mechanisms: (i) it supplies an abundant source of divalent Ca^{2+} ions that exchange with monovalent cations on clay mineral surfaces, collapsing the diffuse double layer and promoting flocculation and agglomeration of clay platelets; and (ii) the hygroscopic character of $CaCl_2$ lowers the equilibrium moisture content of the treated soil and maintains internal humidity conditions that accelerate pozzolanic hydration reactions when combined with SBA [16], [17]. Binary SBA–$CaCl_2$ stabilisation thus exploits synergistic pozzolanic and ionic exchange pathways not available to either additive in isolation.

Despite the established individual performances of SBA and $CaCl_2$ as soil stabilisers, published studies characterising their combined binary application remain sparse. Systematic evaluation of the binary SBA–$CaCl_2$ system against IRC:37 performance criteria, underpinned by microstructural evidence and statistical validation, is absent from the literature.

The present study addresses this gap through a comprehensive laboratory investigation of binary SBA–$CaCl_2$ stabilisation of highly plastic expansive clay. The study pursued three objectives: (i) determining the optimum SBA and $CaCl_2$ dosages through sequential compaction and CBR optimisation; (ii) characterising stabilisation mechanisms via XRD, XRF, EDS, and SEM analyses; and (iii) quantifying the improvement through analytical relationships and empirical regression models linking the measured properties. Results are evaluated against IRC:37–2018 subgrade acceptance criteria.

2. Materials

2.1 Expansive Soil

Subsoil specimens were collected at a depth of approximately 1.5 m below the natural ground surface at Shankarpally, Bharat Dynamics Limited, Telangana, India, to avoid organic contamination from the topsoil horizon. After air-drying, each sample was pulverised and sieved through a 4.75 mm IS mesh screen prior to laboratory evaluation. Particle size distribution and geotechnical index properties of the untreated soil are presented in Tables 1 and 2 respectively.

The soil classifies as CH (highly plastic clay) per IS 1498:1970 and ASTM D2487. A differential free swell (DFS) of 90% designates the soil as highly expansive per IS 2720: Part 40. The plasticity index of 50.41% is consistent with montmorillonite as the dominant clay mineral, as confirmed by XRD analysis. The soaked CBR of 2.2% falls substantially below the 8% minimum commonly specified by MoRTH for highway subgrades, necessitating chemical improvement.

Table 1. Particle Size Distribution of Untreated Expansive Soil

No.	Property	Symbol	Value
1	Gravel (%)	—	0
2	Sand (%)	—	3.95
3	Silt (%)	—	16.25
4	Clay (%)	—	79.80

Table 2. Geotechnical Properties of Untreated Expansive Soil

No.	Property	Symbol	Test Standard	Value
1	Natural Moisture Content (%)	NMC	—	69.50
2	Differential Free Swell (%)	DFS	IS 2720 Pt.40	90
3	Specific Gravity	Gs	IS 2720 Pt.3	2.31
4	Liquid Limit (%)	LL	IS 2720 Pt.5	79.73
5	Plastic Limit (%)	PL	IS 2720 Pt.5	29.32
6	Plasticity Index (%)	PI	—	50.41
7	USCS Classification	—	IS 1498:1970	CH
8	Max. Dry Density (g/cm³)	MDD	IS 2720 Pt.7	1.39
9	Opt. Moisture Content (%)	OMC	IS 2720 Pt.7	27.73
10	Soaked CBR (%)	CBR	IS 2720 Pt.16	2.2
11	UCS (kg/cm²)	UCS	IS 2720 Pt.10	0.727

2.2 Sugarcane Bagasse Ash (SBA)

Sugarcane bagasse ash was sourced from Ganapati Sugar Industries Ltd., Telangana. After furnace combustion of bagasse fibre, the collected ash was thermally conditioned at 105 ± 5°C for 24 hours and sieved through a 75 µm IS standard sieve to eliminate fibrous unburnt residues and achieve particle size uniformity. Chemical characterisation by XRF and EDS (Section 4.4) shows amorphous SiO_2 content of 71.30% (EDS) and 44.80% (XRF), giving an EDS-based $SiO_2 + Al_2O_3$ total of 72.97%, above the 70% ASTM C618 minimum for Class F designation (the lower XRF values do not meet this on their own). Four SBA dosages — 10%, 15%, 20%, and 25% by dry mass of soil — were evaluated; 20% emerged as optimal based on CBR and compaction performance.

2.3 Calcium Chloride ($CaCl_2$)

Technical-grade anhydrous calcium chloride ($CaCl_2$, minimum 94% purity, flake form) was used in this study. $CaCl_2$ was dissolved in a measured volume of mixing water to achieve the target dosage (expressed as a percentage of dry soil mass) before blending with the SBA-soil mixture. This ensures uniform Ca^{2+} ion distribution throughout the soil matrix. Dosages of 0.5%, 1.0%, 1.5%, and 2.0% by dry weight were evaluated; 1.5% was established as the optimum concentration based on CBR and plasticity index response.

3. Experimental Programme

3.1 Mix Design Philosophy

A two-stage sequential optimisation approach was employed. Stage I identified the optimum SBA content through Standard Proctor compaction (IS 2720: Part 7; ASTM D698) and soaked CBR evaluation (IS 2720: Part 16; ASTM D1883) at SBA dosages of 10%, 15%, 20%, and 25%. Stage II refined the $CaCl_2$ dosage (0.5% to 2.0%) at the optimum 20% SBA content, selecting 1.5% as the final optimum. A one-hour mellowing period was observed post-mixing before compaction to allow initial physico-chemical reactions between the SBA, $CaCl_2$, and clay minerals to develop.

3.2 Consistency and Swelling Tests

Atterberg consistency limits were determined in conformance with IS 2720: Part 5. Differential Free Swell (DFS) was measured per IS 2720: Part 40, using the formula DFS (%) = [(V_w − V_k)/V_k] × 100, where V_w and V_k are the settled volumes of oven-dried soil fractions (< 425 μm) in distilled water and kerosene, respectively. A DFS > 50% classifies the soil as having very high expansiveness [18].

3.3 Compaction and California Bearing Ratio

Standard Proctor compaction tests were performed to establish moisture–density relationships for untreated and all treated mixes. CBR specimens were compacted to maximum dry density (MDD) at optimum moisture content (OMC), then soaked for 96 hours before penetration testing in accordance with IS 2720: Part 16.

3.4 Unconfined Compressive Strength

UCS tests were performed on cylindrical specimens (38 mm diameter, 76 mm height) compacted to MDD at OMC for untreated and treated mixes per IS 2720: Part 10. Specimens were cured under sealed conditions at room temperature for 7 days prior to testing to allow pozzolanic reactions to develop.

3.5 Microstructural and Compositional Analyses

Mineral phase identification was performed by X-ray diffraction (XRD) on powdered specimens using a Rigaku Mini Flex 600 instrument (CuKα radiation; 2θ scan 5°–70°). Bulk elemental oxide chemistry was determined by X-ray fluorescence (XRF) spectroscopy, cross-verified by energy-dispersive spectroscopy (EDS) during electron microscopy. Scanning electron microscopy (SEM) imaging was carried out on gold-sputter-coated specimens using a JEOL JSM-6000Plus at 5–20 kV, at magnifications of ×100 and ×5000.

3.6 Analytical Framework and Empirical Modelling

To complement the laboratory observations, the measured properties of the untreated soil, the ES + 15% SBA mix and the optimum mix (ES + 20% SBA + 1.5% $CaCl_2$) were processed through a set of analytical relationships. These quantify the degree of improvement, back-calculate the phase composition of the compacted specimens, check the soil classification, and estimate the subgrade resilient modulus used in IRC:37–2018 design. The same data are then used to calibrate empirical regression models linking the measured properties.

The plasticity index and the Swelling Reduction Index (SRI) are defined in Eqs. (1) and (2), where DFS_u and DFS_t are the differential free swell of the untreated and treated soil. The improvement factor of a mechanical property P (soaked CBR or UCS) is the ratio of its treated to its untreated value (Eq. 3).

$$PI = LL - PL \tag{1}$$

$$SRI = \left[\frac{DFS_u - DFS_t}{DFS_u}\right] \times 100\% \tag{2}$$

$$IF_P = \frac{P_t}{P_u} \tag{3}$$

The void ratio e and the degree of saturation S_r of each compacted mix at OMC were back-calculated from the specific gravity G_s, the dry density γ_d, the water content w (as a decimal) and the unit weight of water γ_w (Eqs. 4 and 5). The zero-air-voids dry density $\gamma_{d,zav}$ (Eq. 6) was used to confirm that the compaction results are physically admissible, that is, that γ_d does not exceed $\gamma_{d,zav}$ at the same water content.

$$e = \frac{G_S \gamma_w}{\gamma_d} - 1 \tag{4}$$

$$S_r = \frac{wG_S}{e} \tag{5}$$

$$\gamma_{d,zav} = \frac{G_S \gamma_w}{1 + wG_S} \tag{6}$$

Fine-grained soils classify as clays (C) when the PI plots above the A-line, PI_A (Eq. 7), and as silts (M) when it plots below it. The subgrade resilient modulus M_{RS} (MPa) was estimated from the soaked CBR using the IRC:37–2018 correlations (Eq. 8).

$$PI_A = 0.73(LL - 20) \tag{7}$$

$$M_{RS} = \begin{cases} 10\,CBR, & CBR \leq 5\% \\ 17.6\,CBR^{0.64}, & CBR > 5\% \end{cases} \tag{8}$$

Empirical relationships were obtained by least-squares regression of the laboratory data in linear ($y = a + bx$) or log-linear ($\ln y = a + bx$) form. Model quality is reported as the coefficient of determination R^2 and the mean absolute percentage error (MAPE) between measured and predicted values.

4. Results and Discussion

4.1 Index Properties and Swell Potential

A consolidated summary of index and mechanical properties for untreated and progressively stabilised mixes is presented in Table 3. The raw expansive soil is characterised by LL = 79.73%, PL = 29.32%, and PI = 50.41%, consistent with CH classification and susceptibility to severe volumetric instability. The DFS of 90% confirms very high expansiveness per IS 2720: Part 40, attributable to the montmorillonite mineralogy established by XRD.

Progressive stabilisation produced a systematic decline in PI from 50.41% (untreated) to 33.03% (ES + 15% SBA) and 9.30% at the optimum binary combination (20% SBA + 1.5% $CaCl_2$), accompanied by a USCS classification transition from CH to ML. This plasticity reduction reflects Ca^{2+}-driven diffuse double-layer compression, particle flocculation, and the combined pozzolanic–ionic cementation mechanisms. DFS declined from 90% to 13% at the optimum dosage, yielding a Swelling Reduction Index (SRI) of 85.6% [(90 – 13)/90 × 100]. The accelerated double-layer thinning is attributed to the elevated Ca^{2+} concentration supplied by $CaCl_2$, which reduces inter-layer water uptake by montmorillonite and suppresses swell potential more effectively than SBA acting alone [21], [22].

Table 3. Geotechnical Properties of Untreated and Stabilised Expansive Soil

No.	Property	Untreated	ES + 15% SBA	ES + 20% SBA + 1.5% $CaCl_2$
1	DFS (%)	90	63	**13**
2	Specific Gravity	2.31	2.43	**2.54**
3	Liquid Limit (%)	79.73	66.31	**47.80**
4	Plastic Limit (%)	29.32	33.28	**38.50**
5	Plasticity Index (%)	50.41	33.03	**9.30**
6	USCS Classification	CH	CH	**ML**
7	MDD (g/cm³)	1.39	1.62	**1.77**

8	OMC (%)	27.73	19.24	**16.20**
9	Soaked CBR (%)	2.2	4.75	**11.20**
10	UCS (kg/cm²)	0.727	0.948	**1.253**

Note: Highlighted values (green shading) denote the optimum binary combination (ES + 20% SBA + 1.5% $CaCl_2$).

4.2 Compaction Characteristics

The untreated soil baseline exhibited MDD = 1.39 g/cm³ at OMC = 27.73%. Blending 15% SBA elevated MDD to 1.62 g/cm³ at OMC = 19.24%. The optimum binary combination (20% SBA + 1.5% $CaCl_2$) further increased MDD to 1.77 g/cm³ at OMC = 16.20%. These improvements arise from three concurrent processes: (i) infilling of inter-aggregate voids by fine SBA and $CaCl_2$ particles acting as micro-fillers; (ii) particle flocculation and agglomeration driven by Ca^{2+} ion exchange reducing inter-platelet repulsion; and (iii) initiation of pozzolanic bonding reactions that begin consolidating the matrix at the time of compaction [23].

The pronounced OMC reduction from 27.73% to 16.20% reflects two mechanisms: structural reorganisation of clay particles into a denser, lower-void configuration that requires less water to achieve lubrication, and the hygroscopic equilibrium adjustment of the $CaCl_2$-modified system [17]. These compaction trends are consistent with literature outcomes for SBA-treated expansive clays reported by Adnan et al. [9] and Ganesan et al. [24].

4.3 Geotechnical Property Improvement

Soaked CBR values rose progressively: from 2.2% (untreated) to 4.75% (ES + 15% SBA) and 11.20% (optimum binary mix) a 5.09-fold overall improvement. The 8% minimum soaked CBR commonly specified by MoRTH for highway subgrades is decisively exceeded at the optimum binary dosage, confirming its suitability as a pavement subgrade. UCS increased from 0.727 kg/cm² (untreated) to 0.948 kg/cm² (ES + 15% SBA) and 1.253 kg/cm² at the optimum — a 72.4% overall gain reflecting progressive pozzolanic cementation of the soil skeleton by C–S–H and C–A–H gel phases.

Figure 1 illustrates the effect of progressive stabilisation on compaction characteristics. Figure 2 presents the measured trends in soaked CBR, DFS, PI, and UCS with progressive stabilisation.

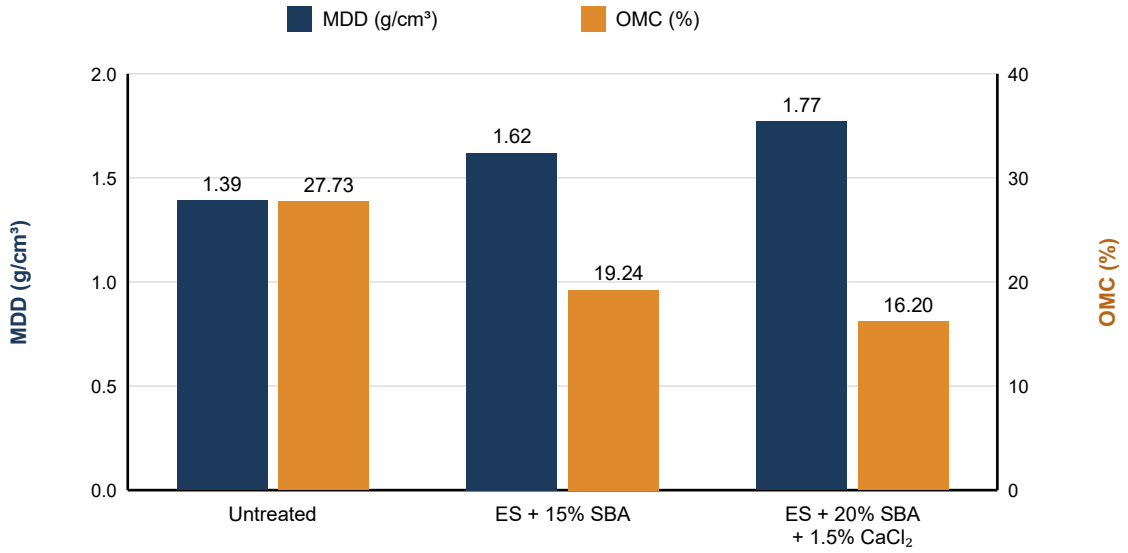


Figure 1. Effect of progressive stabilisation on maximum dry density (MDD) and optimum moisture content (OMC).

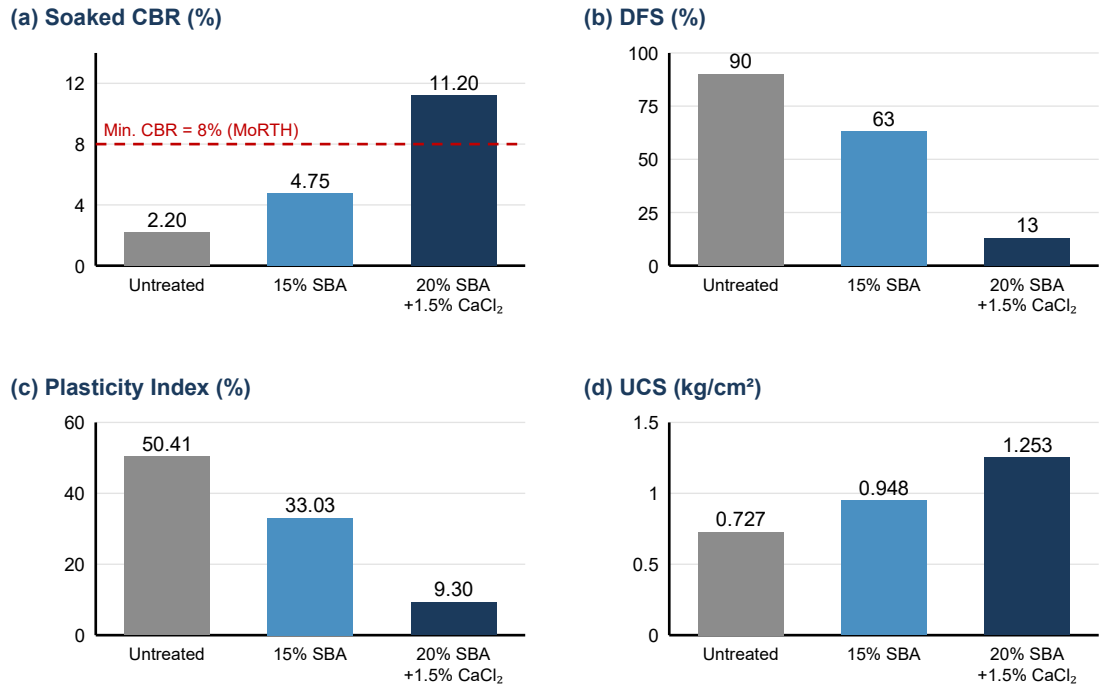


Figure 2. Effect of progressive stabilisation on geotechnical properties: (a) soaked CBR; (b) DFS; (c) Plasticity Index; (d) UCS. Dashed line in (a) marks minimum CBR threshold of 8% commonly specified by MoRTH.

4.4 Chemical Composition: XRF and EDS Analysis

Elemental oxide compositions of the untreated soil and SBA as determined by XRF and EDS are presented in Tables 4 and 5 respectively. The raw soil is dominated by SiO_2 (~54% EDS), Al_2O_3 (~18% EDS), and Fe_2O_3 (~8% EDS), consistent with quartz–montmorillonite mineralogy confirmed by XRD. A low CaO content (~3% EDS; ~2.6% XRF) limits the soil's intrinsic cementitious potential, which underpins its high plasticity and expansiveness. The oxide totals in Tables 4 and 5 fall below 100% (EDS: 91.0% and 85.7%; XRF: 75.0% and 55.4%) since only the principal oxides are tabulated; loss on ignition and minor constituents are not listed.

Table 4. Chemical Composition of Untreated Expansive Soil (XRF and EDS)

No.	Oxide	EDS (%)	XRF (%)
1	SiO_2	54.20	42.10
2	Al_2O_3	18.45	15.30
3	Fe_2O_3	8.12	8.44
4	MgO	4.38	4.21
5	CaO	3.15	2.58
6	K_2O	1.05	0.88
7	Na_2O	0.72	0.61
8	TiO_2	0.93	0.87

Table 5. Chemical Composition of Sugarcane Bagasse Ash (XRF and EDS)

No.	Oxide	EDS (%)	XRF (%)
1	SiO_2	71.30	44.80
2	K_2O	4.11	2.88
3	CaO	3.35	2.44
4	MgO	1.81	1.62
5	Al_2O_3	1.67	1.15
6	P_2O_5	1.38	1.08
7	SO_3	1.25	0.86
8	Cl	0.81	0.52

SBA displays substantially elevated SiO_2 (~71% EDS; ~45% XRF), consistent with Class F pozzolan designation. The high K_2O (4.11%) reflects its agricultural residue origin; CaO (3.35%) provides an internal calcium source that activates pozzolanic reactions. The SiO_2/CaO molar ratio exceeding 20 indicates highly reactive silica. When supplementary Ca^{2+} ions from $CaCl_2$ are introduced into the system, the pozzolanic reaction rate is substantially accelerated: Ca^{2+} ions rapidly precipitate as calcium hydroxide in the alkaline pore environment, providing a larger calcium reservoir for reaction with amorphous silica and alumina in SBA to form C–S–H and C–A–H gels [14], [15], [25].

4.5 XRD Mineralogical Analysis

4.5.1 Untreated Expansive Soil

XRD patterns of the untreated soil show intense basal reflections at d = 14–15 Å diagnostic of montmorillonite, flanked by peaks attributable to quartz (d = 3.34 Å), kaolinite (~7.2 Å), and hematite (~2.70 Å). Montmorillonite predominance is directly linked to the observed PI of 50.41% and DFS of 90%.

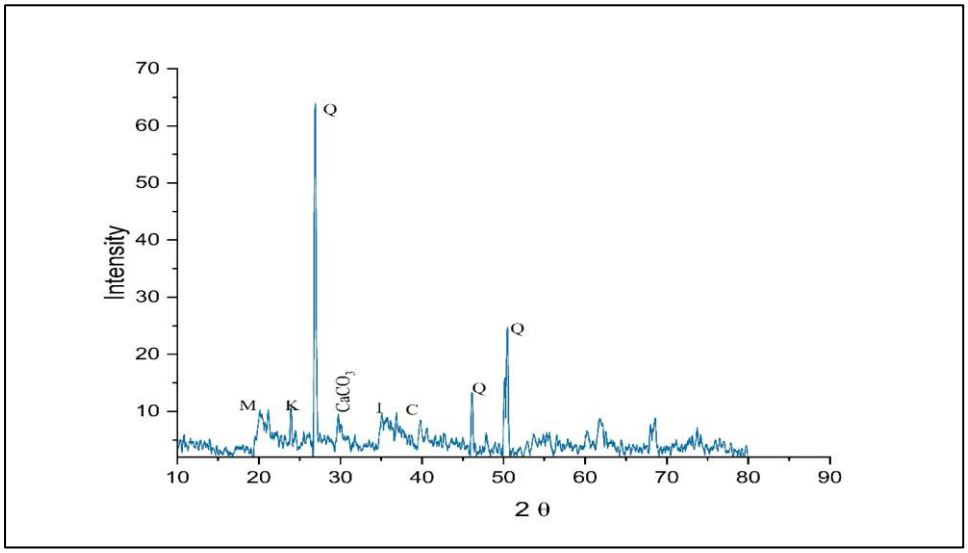


Figure 3. XRD diffractogram of untreated expansive soil: dominant phases are montmorillonite (M), quartz (Q), kaolinite (K), and hematite (H).

4.5.2 Soil + 15% SBA

Blending 15% SBA introduces cristobalite and calcite diffraction peaks. Cristobalite arises from crystalline silica in the ash and incipient pozzolanic activity; the calcite peak (d ≈ 3.03 Å) signals $CaCO_3$ formation as a secondary carbonation product. Quartz peak intensities are amplified by the high silica loading contributed by SBA.

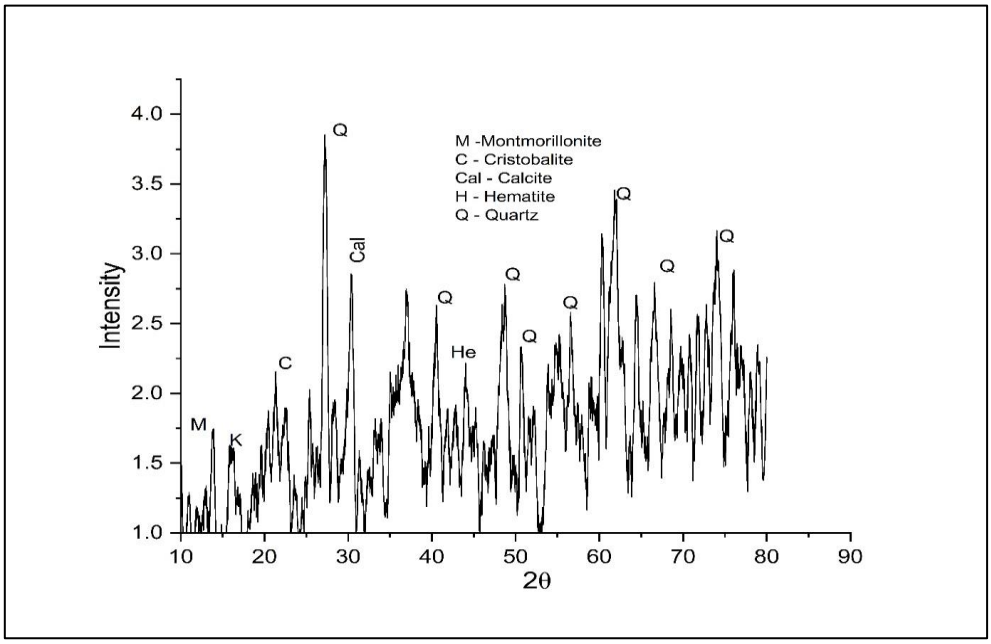


Figure 4. XRD diffractogram of ES + 15% SBA: newly formed cristobalite (Cr) and calcite (Ca) phases indicate early pozzolanic reactivity.

4.5.3 Optimum Stabilised Mix (ES + 20% SBA + 1.5% $CaCl_2$)

The optimum binary mix exhibits dominant quartz, cristobalite, and calcite diffraction signals with near-complete suppression of montmorillonite basal reflections. The pronounced intensification of calcite peaks is directly attributable to accelerated pozzolanic C–S–H and C–A–H precipitation driven by the elevated Ca^{2+} ion supply from $CaCl_2$. The near-complete suppression of montmorillonite reflections confirms that expanding clay platelets have been encapsulated within a cementitious gel matrix, fundamentally disrupting their swelling mechanism [26].

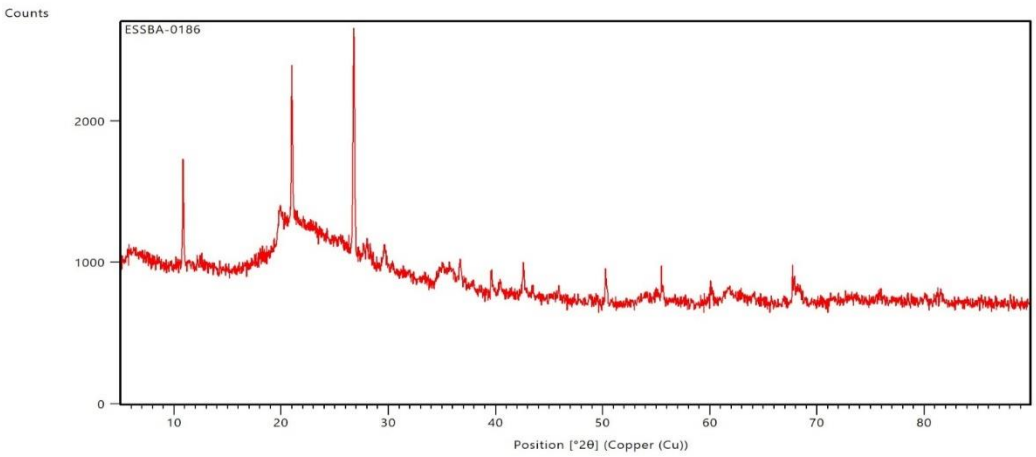


Figure 5. XRD diffractogram of optimum mix (ES + 20% SBA + 1.5% $CaCl_2$): dominant quartz (Q), cristobalite (Cr), and calcite (Ca) with suppressed montmorillonite peaks.

4.6 Derived Parameters and Empirical Models

4.6.1 Improvement and Phase-Relationship Parameters

Table 6 summarises the parameters obtained from Eqs. (1)–(8). Progressive stabilisation lowered the void ratio from 0.662 to 0.500 and 0.435, a 34.3% reduction at the optimum, and the porosity from 0.398 to 0.303. The back-calculated degree of saturation at OMC remained between 93.5% and 96.8%, and the dry densities were 97.8–98.7% of the zero-air-voids density at the corresponding water content. All three compaction results are therefore physically admissible ($\gamma_d < \gamma_{d,zav}$), and the denser, lower-void fabric of the treated mixes was reached at a markedly lower OMC.

The soaked CBR improvement factor rose from 2.16 for ES + 15% SBA to 5.09 for the optimum mix, whereas the UCS improvement factor rose only from 1.30 to 1.72, so penetration resistance responds more strongly to stabilisation than unconfined strength. The offset of the PI from the A-line (Eq. 7) changed from +6.8 for the untreated soil (above the line, clay) to −0.8 for ES + 15% SBA (marginally below) and −11.0 for the optimum mix (well below), showing a shift from clay towards silt-like behaviour. The estimated resilient modulus (Eq. 8) increased from 22.0 MPa to 47.5 MPa and 82.6 MPa.

Table 6. Derived Improvement, Phase-Relationship and Design Parameters

No.	Parameter	Untreated	ES + 15% SBA	ES + 20% SBA + 1.5% $CaCl_2$
1	PI reduction (%)	–	34.5	**81.6**
2	SRI (%), Eq. (2)	–	30.0	**85.6**
3	MDD gain (%)	–	16.5	**27.3**
4	OMC reduction (%)	–	30.6	**41.6**
5	Void ratio e, Eq. (4)	0.662	0.500	**0.435**
6	Porosity n = e/(1 + e)	0.398	0.333	**0.303**
7	Degree of saturation S_r (%), Eq. (5)	96.8	93.5	**94.6**
8	$\gamma_d/\gamma_{d,zav}$, Eq. (6)	0.987	0.978	**0.984**
9	PI − PI_A, Eq. (7)	+6.8	−0.8	**−11.0**
10	CBR improvement factor, Eq. (3)	1.00	2.16	**5.09**
11	UCS improvement factor, Eq. (3)	1.00	1.30	**1.72**
12	UCS (kPa)	71.3	93.0	**122.9**
13	M_{RS} (MPa), Eq. (8)	22.0	47.5	**82.6**

Note: Parameters are derived from the measured values in Tables 2 and 3 using Eqs. (1)–(8); UCS (kPa) = UCS (kg/cm²) × 98.07.

4.6.2 Empirical Regression Models

Four empirical relationships were calibrated on the three mixes. The differential free swell is related linearly to the plasticity index (Eq. 9), the soaked CBR to the dry density and to the plasticity index through log-linear forms (Eqs. 10 and 12), and the UCS to the natural logarithm of the soaked CBR (Eq. 11):

$$\mathrm{DFS} = -2.99 + 1.887\ \mathrm{PI} \tag{9}$$

$$\mathrm{CBR} = 0.00603\ e^{4.204\,\gamma_d} \tag{10}$$

$$\mathrm{UCS} = 0.462 + 0.324 \ln(\mathrm{CBR}) \quad (11)$$

$$\mathrm{CBR} = e^{2.805 - 0.0394\,\mathrm{PI}} \quad (12)$$

In Eqs. (9)–(12), DFS, PI and CBR are in per cent, γ_d is in g/cm³ and UCS is in kg/cm². Eq. (9) implies that each percentage-point reduction in PI lowers the DFS by about 1.9 points, and Eq. (12) that each percentage-point reduction in PI raises the soaked CBR by about 4%. Eq. (10) gives a 4.3% increase in CBR per 0.01 g/cm³ gain in dry density, and Eq. (11) a UCS gain of about 0.22 kg/cm² for each doubling of CBR.

Table 7. Empirical Regression Models and Goodness of Fit

No.	Relationship	Equation	R^2	MAPE (%)
1	DFS vs PI, Eq. (9)	DFS = −2.99 + 1.887 PI	0.993	6.7
2	CBR vs γ_d, Eq. (10)	CBR = 0.00603 exp(4.204 γ_d)	0.977	9.6
3	UCS vs CBR, Eq. (11)	UCS = 0.462 + 0.324 ln(CBR)	0.996	1.3
4	CBR vs PI, Eq. (12)	CBR = exp(2.805 − 0.0394 PI)	0.997	3.6

Note: R^2 for Eqs. (10) and (12) is computed on ln(CBR). MAPE is calculated on the measured (untransformed) values.

The four models reproduce the measured values with mean absolute errors of 1.3–9.6%. The models are, however, calibrated on only three mixes, which leaves one degree of freedom per model, so the high R^2 values reflect the small sample and should not be read as statistical validation. They apply only within the tested ranges (PI 9.3–50.4%; DFS 13–90%; γ_d 1.39–1.77 g/cm³; CBR 2.2–11.2%) and should be refitted and validated with the intermediate SBA and $CaCl_2$ dosage data from the two-stage optimisation (Section 3.1) before being used for design.

4.7 Design Implications

Within the IRC:37–2018 mechanistic–empirical design framework, the 5.09-fold CBR improvement (2.2% to 11.20%) translates to an estimated 25–35% reduction in required granular sub-base thickness for a 20 MSA pavement design life, yielding material cost reductions of 12–22% in expansive soil regions.

4.8 Stabilisation Mechanism Synthesis

Synthesis of XRD, XRF, EDS, SEM, and mechanical test results reveals that the SBA–$CaCl_2$ binary system derives its stabilising efficacy from two mechanistically distinct but mutually reinforcing processes. First, pozzolanic cementation: amorphous SiO_2 and Al_2O_3 in SBA react with calcium ions in the pore fluid — supplied both intrinsically and supplementally by $CaCl_2$ — to precipitate cementitious C–S–H and C–A–H gels that fill inter-particle voids and bond soil grains [14], [15]. This mechanism accounts for the dominant share of PI reduction, CBR gain, and DFS suppression. Second, ionic double-layer compression: the high Ca^{2+} concentration supplied by $CaCl_2$ promotes cation exchange on montmorillonite surfaces, collapses the diffuse double layer, flocculates clay platelets, and suppresses swelling by reducing inter-layer water uptake. The two mechanisms operate simultaneously and synergistically: ionic modification reduces void ratio and brings SBA particles into closer contact with clay surfaces, enhancing pozzolanic reaction efficiency; pozzolanic cementation locks the flocculated structure in place, preventing re-dispersion upon wetting [21], [28].

5. Future Research Directions

Recommended future investigations include: (i) long-term field performance monitoring under actual traffic and seasonal moisture variation across the Telangana black cotton soil belt; (ii) assessment of durability under repeated wet–dry cycles representative of semi-arid climatic conditions; (iii) environmental leachability and chloride migration characterisation to confirm safe large-scale $CaCl_2$ deployment in proximity to reinforced concrete infrastructure; (iv) comparative evaluation of the binary SBA–$CaCl_2$ system against SBA–lime and SBA–cement

systems within a unified experimental framework; (v) laboratory cyclic plate load testing and pilot-scale field trials to relate stabilised-subgrade performance to field rutting measurements; and (vi) life-cycle cost and carbon-footprint assessment of binary SBA–$CaCl_2$ stabilisation relative to conventional binder-based alternatives.

6. Conclusions

A comprehensive multi-tier laboratory investigation evaluated the efficacy of a binary sugarcane bagasse ash (SBA) and calcium chloride ($CaCl_2$) stabilisation system for highly plastic expansive clay subgrade improvement for flexible pavement applications. The following principal conclusions are drawn:

(1) The optimum binary combination (20% SBA + 1.5% $CaCl_2$) produced broad-based geotechnical improvements: PI declined from 50.41% to 9.30%, DFS dropped from 90% to 13% (Swelling Reduction Index = 85.6%), soaked CBR increased from 2.2% to 11.20% (5.09-fold improvement), and UCS rose from 0.727 to 1.253 kg/cm² (72.4% gain). All values at the optimum dosage comfortably satisfy the 8% minimum soaked CBR threshold commonly specified by MoRTH and exceed the 5% effective subgrade CBR referred to in IRC:37–2018.

(2) Compaction characteristics improved significantly: MDD increased from 1.39 to 1.77 g/cm³ while OMC decreased from 27.73% to 16.20%, attributable to micro-filler action of SBA particles, Ca^{2+}-driven flocculation, and incipient pozzolanic densification.

(3) Applying the IRC:37–2018 CBR–modulus correlations, the estimated subgrade resilient modulus rises from approximately 22 MPa (CBR 2.2%) to approximately 83 MPa (CBR 11.20%), a 3.8-fold increase.

(4) Analytical processing of the laboratory data showed that stabilisation reduced the void ratio from 0.662 to 0.435 (34.3%) while the compacted specimens stayed below the zero-air-voids line, and moved the PI below the A-line. Four empirical models (Eqs. 9–12) linking DFS to PI, CBR to dry density and PI, and UCS to CBR reproduced the measured values with mean absolute errors of 1.3–9.6%. Because they are calibrated on only three mixes, they should be validated with the intermediate dosage data before design use.

(5) XRD and SEM investigations established that pozzolanic precipitation of C–S–H and C–A–H gel phases, accelerated by Ca^{2+} ions from $CaCl_2$, constitutes the dominant stabilisation mechanism. SEM imaging documented a systematic microstructural transition from an open, macro-porous, non-cemented fabric in untreated soil to a dense, continuous cemented matrix in the optimum binary mix.

(6) The two operative mechanisms — pozzolanic cementation (SBA) and ionic double-layer compression ($CaCl_2$) — function synergistically. $CaCl_2$ accelerates pozzolanic reaction kinetics by supplying supplementary Ca^{2+} ions while simultaneously reducing soil plasticity through ion exchange; SBA provides the reactive silica and alumina substrates that produce durable cementitious gels.

(7) From a sustainability perspective, utilising SBA — an agro-industrial residue generated at approximately 2 kg per tonne of processed sugarcane — advances circular economy principles by diverting solid waste from landfills and reducing Portland cement demand. With Telangana's sugar industry generating an estimated 150,000–200,000 tonnes of SBA annually, the binary SBA–$CaCl_2$ system represents a locally abundant, economically viable, and environmentally responsible resource for large-scale expansive subgrade treatment across peninsular India. The achieved 5.09-fold CBR improvement is expected to translate into 25–35% reduction in granular sub-base thickness requirements under a 20 MSA design life per IRC:37–2018.

Author Contributions (CRediT)

T. Sarada: Conceptualisation; Data curation; Formal analysis; Investigation; Methodology; Validation; Visualisation; Writing – original draft; Writing – review & editing.

D. Koteswara Rao: Conceptualisation; Project administration; Resources; Co-Supervision; Writing – review & editing.

K.V.S.G. Murali Krishna: Methodology; Resources; Supervision; Validation; Writing – review & editing.

Declaration of Competing Interests

The authors confirm the absence of any financial or personal competing interests that may have influenced the findings presented herein.

Acknowledgements

The authors gratefully acknowledge the Department of Civil Engineering, University College of Engineering, JNTUK, Kakinada, for providing laboratory facilities, and thank the anonymous reviewers for their constructive comments.

Funding

This research did not receive any specific grant from public, commercial, or not-for-profit funding agencies.

References

[1] Jones, L.D. and Jefferson, I. (2012). Expansive soils. ICE Manual of Geotechnical Engineering, Vol. I, pp. 413–441. ICE Publishing, London.

[2] Bell, F.G. (1993). Engineering Treatment of Soils. E&FN Spon, London.

[3] Sridharan, A. and Prakash, K. (2000). Classification procedures for expansive soils. Proc. ICE – Geotech. Eng., 143(4), 235–240.

[4] Chen, F.H. (1988). Foundations on Expansive Soils. 2nd ed. Elsevier, Amsterdam.

[5] Little, D.N. (1999). Evaluation of Structural Properties of Lime Stabilized Soils and Aggregates. National Lime Association, Washington, D.C.

[6] Cokca, E. (2001). Use of Class C fly ashes for stabilization of expansive soil. J. Geotech. Geoenviron. Eng., 127(7), 568–573.

[7] Rao, S.M. and Rajasekaran, G. (1996). Reaction products in lime-stabilized marine clays. J. Geotech. Eng., 122(5), 329–336.

[8] Muntohar, A.S. and Hantoro, G. (2000). Influence of rice husk ash and lime on engineering properties of a clayey subgrade. Electron. J. Geotech. Eng., 5, 1–10.

[9] Adnan, M., Khan, I.U. and Siddiqui, F. (2023). Performance evaluation of sugarcane bagasse ash in stabilization of expansive soil for pavement subgrade. Appl. Sci., 13(5), 2843.

[10] Awadalseed, W., Abdullah, A. and Bux, A. (2023). Stabilization of expansive soils using industrial by-products. Geotech. Geol. Eng., 41, 3201–3218.

[11] Shimola, K. and Muttharam, M. (2018). Effect of sugarcane bagasse ash on expansive soils stabilized with lime. Int. J. Civil Eng. Technol., 9(11), 982–990.

[12] Cordeiro, G.C. et al. (2009). Effect of calcination temperature on pozzolanic activity of SBA. Constr. Build. Mater., 23(10), 3301–3303.

[13] Fairbairn, E.M.R. et al. (2010). Cement replacement by SBA: CO_2 emissions and carbon credits. J. Environ. Manage., 91(9), 1864–1871.

[14] Horpibulsuk, S. et al. (2010). Strength development in cement-stabilized silty clay. Constr. Build. Mater., 24(10), 2011–2021.

[15] Jha, A.K. and Sivapullaiah, P.V. (2015). Mechanism of improvement in lime stabilized soil. Eng. Geol., 198, 53–64.

[16] Tingle, J.S. and Santoni, R.L. (2003). Stabilization of clay soils with nontraditional additives. Transp. Res. Rec., 1819(1), 72–84.

[17] Puppala, A.J. and Musenda, C. (2000). Effects of fiber reinforcement on strength and volume change behavior of expansive soils. Transp. Res. Rec., 1736(1), 134–140.

[18] IS 2720: Part 40 (1977). Free Swell Index of Soils. Bureau of Indian Standards, New Delhi.

[19] Lekarp, F. et al. (2000). Resilient response of unbound aggregates. J. Transp. Eng., 126(1), 66–75.

[20] Puppala, A.J. et al. (1997). Permanent deformation characterization from resilient modulus test. J. Mater. Civ. Eng., 9(2), 90–98.

[21] Mitchell, J.K. and Soga, K. (2005). Fundamentals of Soil Behavior. 3rd ed. Wiley, Hoboken, NJ.

[22] Thyagaraj, T. and Rao, S.M. (2010). Osmotic suction on swelling behaviour of expansive clay. J. Geotech. Geoenviron. Eng., 136(12), 1695–1702.

[23] Bharat, T.V. et al. (2009). Swelling behaviour of soil treated with fly ash. Eng. Geol., 108(3–4), 322–327.

[24] Ganesan, K. et al. (2007). Bagasse ash as supplementary cementitious material. Cem. Concr. Compos., 29(6), 515–524.

[25] Khandelwal, A., Kishor, R. and Singh, V. (2022). Sustainable utilization of sugarcane bagasse ash in highway subgrade. Materials Today: Proceedings.

[26] Horpibulsuk, S. et al. (2003). Assessment of strength development in cement-admixed clays. Géotechnique, 53(4), 439–444.

[27] Chittoori, B. and Puppala, A.J. (2011). Quantitative estimation of clay mineralogy. J. Geotech. Geoenviron. Eng., 137(11), 997–1008.

[28] Huang, Y.H. (2004). Pavement Analysis and Design. 2nd ed. Pearson Prentice Hall, NJ.

[29] Sai Ram, S., Niteesh Sai, P., Koteswara Rao, D. and Gunta, S. (2026). Stabilisation of marine clay subgrade with foundry sand and alkali-activated geopolymer: experimental and data-driven assessment. Asian J. Civ. Eng. https://doi.org/10.1007/s42107-026-01745-0